Structural and Electrical Characteristics of Sol-Gel ZnO Films on Black Silicon

Gagik Ayvazyan
National Polytechnic University of Armenia, Yerevan, Armenia
agagarm@gmail.com (corresponding author)

Laura Lakhoyan
National Polytechnic University of Armenia, Yerevan, Armenia
llakhoyan@mail.ru

Alina Semchenko
Skorina Gomel State University, Gomel, Belarus
alina@gsu.by

Received: 14 March 2025 | Revised: 14 April 2025 | Accepted: 19 April 2025

 DOI: https://doi.org/10.48084/etasr.10942

ABSTRACT

In this work, zinc oxide (ZnO) films were deposited on silicon (Si) substrates with and without Black Silicon (BS) using the sol-gel spin-coating method. The nanotexturing of the Si surface was performed via reactive ion etching, resulting in the formation of a conical nanoneedle array that enhanced light trapping efficiency. X-ray Diffraction (XRD) analysis confirmed that the ZnO films exhibited a polycrystalline hexagonal wurtzite structure. The formation of n-ZnO/p-Si heterostructures was validated through Scanning Electron Microscopy (SEM), Energy-Dispersive X-ray Spectroscopy (EDS), and current-voltage (I–V) measurements. The incorporation of BS at the heterostructure interface significantly enhances the spectral response across the entire wavelength range due to superior light-trapping properties and an increased contact area at the heterojunction. These findings are highly relevant for the development of photodetectors and other optoelectronic devices based on ZnO and BS.

Keywords-black silicon; sol-gel film; ZnO; morphology; spectral responsivity

I. INTRODUCTION

The unique properties of zinc oxide (ZnO), such as a wide forbidden transition (3.37 eV), high exciton binding energy (60 meV), transparency in the visible range (>80%), piezoelectric characteristics, chemical and thermal stability, and low toxicity, make it a versatile material for a wide range of applications [1, 2]. Various methods are used to obtain ZnO thin films, including thermal evaporation, atomic layer deposition, chemical vapor deposition, pulsed laser deposition, radio-frequency magnetron sputtering, electrochemical deposition, and sol-gel process [3-7]. Among these methods, the sol-gel technology stands out due to several advantages, such as ease of implementation, the ability to precisely control the chemical composition of the films, low equipment cost, and the ability to obtain large-area films with high thickness uniformity [8].

The integration of ZnO with other semiconductors, particularly silicon (Si), offers promising avenues for the development of multifunctional and high-efficiency devices, such as solar cells, photodetectors, light-emitting diodes, sensors, and energy-harvesting systems [9-11]. Research in this field focuses on developing new device architectures, improving material quality, and optimizing the interfaces between ZnO and Si. For this purpose, Si with microtextured surfaces, such as porous Si, is widely used [5, 7, 12-14]. It has already been demonstrated that ZnO/Si heterostructures with microtextured surfaces not only exhibit excellent light trapping behavior, but also provide intense light emission and enhanced light extraction [6, 7, 15, 16].

In recent years, Si with a nanotextured surface, known as BS, has been studied to enhance light absorption [17-20]. BS consists of an array of densely packed cone-shaped nanoneedles, with dimensions smaller than the wavelength of incident light. The ultra-low reflectivity of BS is attributed to the scattering of incident light and the formation of an effective medium with a gradient refractive index along the height of the nanoneedles. In our previous study, it was demonstrated that a nanotextured Si surface significantly reduces reflection and enhances broadband light absorption when combined with films of metal oxides [21]. The use of BS at the ZnO/Si interface can also facilitate the formation of highly efficient heterojunctions, thereby expanding the functionality of photoelectronic devices based on these structures. However, such studies are scarcely reported in the literature.

In this work, ZnO films were deposited on Si substrates with and without BS using the sol-gel spin-coating technique. The resulting nanotextured n-ZnO/p-Si heterostructures exhibited distinct structural and electrical characteristics compared to planar configurations. These findings highlight the strong potential of ZnO/BS heterostructures for future electronic and photonic device applications.

II. EXPERIMENT

The initial substrates used in this study were p-type (boron-doped) single-crystal Si wafers with a (100) crystallographic orientation and a resistivity of 1.0–3.0 Ω·cm. The substrates were first immersed in hydrofluoric acid (HF) for 10 sec and then rinsed with ethanol. For the comparative analysis, experimental ZnO/Si structures with and without BS at the interface (referred to as nanotextured and planar samples, respectively) were fabricated and studied.

BS was formed on one side of the substrates using maskless Reactive Ion Etching (RIE) in an SF_6/O_2 gas mixture. The etching process was conducted at a pressure of 55 mTorr for 10 min, with gas flow rates of 75 cm^3/min for SF_6 and 40 cm^3/min for O_2. After the electrochemical treatment, the working surface of the samples was rinsed with distilled water and dried using nitrogen blow-drying. A detailed description of the BS fabrication procedure is available in [18].

ZnO films were synthesized using the sol-gel spin-coating method. The precursor sol was prepared by dissolving zinc acetate in absolute isopropyl alcohol and aging the solution at room temperature for 48 hours. A thin seed layer was deposited by spin-coating at a substrate rotation speed of 2000 rpm, followed by preliminary drying at 250 °C for 10 min and final heat treatment in a muffle furnace at 450 °C for 60 min. The deposition and drying process was repeated until the desired film thickness was achieved. In the final stage, the samples were placed in a furnace and heated stepwise in 20 °C increments up to 550 °C. After synthesis, the ZnO/Si structures were rinsed with distilled water and dried by purging with nitrogen.

The morphology of the samples, including cross-sectional and top-view features, was examined using a Hitachi S-4800 (Japan) SEM. The elemental composition of the samples was determined via EDS, using a Bruker QUANTAX200 spectrometer (Germany), operating at 10 kV. For structural and phase analysis, a Malvern Panalytical X-ray diffractometer (Netherlands) was employed, utilizing CoKα radiation with a wavelength of 1.542 Å in 2θ mode. To measure the I-V characteristics of the ZnO/Si sandwich structures, ohmic contacts were fabricated on both sides using thermal evaporation of aluminum (Al). The I-V measurements were carried out using an E7-25 voltage source (Belarus). Voltage was applied between the top ZnO contact and the ohmic back contact. In the forward bias configuration, the ohmic back contact was grounded, while the ZnO contact was negatively biased. The measurements were conducted at room temperature in the dark, with a voltage range from –2 to +2 V. Additionally, the spectral responsivity of the samples was evaluated across the 350–1000 nm wavelength range using a Spectroscopic Prism Monochromator (SPM) (Germany).

III. RESULTS AND DISCUSSION

Figure 1 presents representative cross-sectional and top-view SEM images of the studied samples. As seen in Figures 1(a) and 1(b), the RIE process yields a quasi-ordered array of conical nanoneedles on the Si surface, with face inclination angles ranging from 70° to 80°. These nanoneedles are smooth and free of nanowhiskers or nanoclusters, indicating the high isotropy of the etching process. Within microscale regions, the nanoneedles are randomly distributed with narrow interspatial gaps, typically less than 100 nm. The base diameter of the nanoneedles varies between 165 and 205 nm, with an average height of approximately 680 nm. This nanotexturing leads to an estimated ninefold increase in the specific surface area compared to the planar Si substrate.

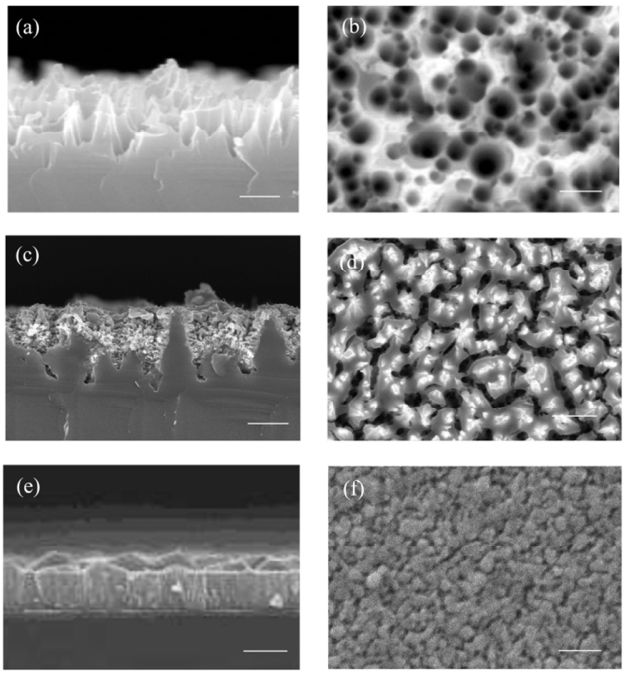

Fig. 1. Cross-sectional (a, c, e) and top (b, d, f) SEM images of BS (a, b), ZnO/Si nanotextured (c, d), and planar (e, f) structures. All scale bars are 500 nm.

On planar Si in Figures 1(e) and 1(f), the deposited ZnO film appears uniform, exhibiting low surface roughness. The film consists of ordered crystallites with a uniform growth direction perpendicular to the Si substrate. In contrast, the ZnO film grown on the nanotextured Si surface displays a fibrous structure, as shown in Figures 1(c) and 1(d). In this case, the fibers grow either from the interneedle space perpendicular to the Si substrate or obliquely from the faces of the nanoneedles. The omnidirectional growth of ZnO on BS is driven by sufficient activation energy, allowing it to occupy the correct nucleation sites along the nanotextured surface [5]. The ZnO layer uniformly penetrates and envelops the BS matrix, forming a conformal coating. The average total thickness of the ZnO film is approximately 530 nm for both planar and nanotextured substrates. Additionally, SEM images reveal the

presence of a denser ZnO seed sublayer, approximately 80 nm thick, at the interface in both sample types.

The XRD patterns of ZnO films deposited on planar and nanotextured Si surfaces are depicted in Figure 2. In both cases, prominent diffraction peaks are observed at 2θ values of 31.95°, 34.64°, 36.42°, 47.87°, 57.16°, and 63.18°, corresponding to the (100), (002), (101), (102), (110), and (103) crystal planes, respectively. These peaks confirm the formation of a polycrystalline hexagonal wurtzite structure of the ZnO phase. The diffraction peak at 68.14° (400) corresponds to the reflection from the Si substrate. This peak is particularly pronounced for the nanotextured sample, indicating effective integration of ZnO into the BS nanoneedle array. The average crystallite size of ZnO was calculated along the (002) direction using the Scherrer formula. The crystallite size was found to be 71.6 nm for the planar surface and 83.4 nm for the nanotextured sample. The increase in crystallite size is likely due to the highly lyophilic nature of BS [22], which promotes larger crystallite formation, similar to the growth process observed in liquid perovskites on nanotextured surfaces [23].

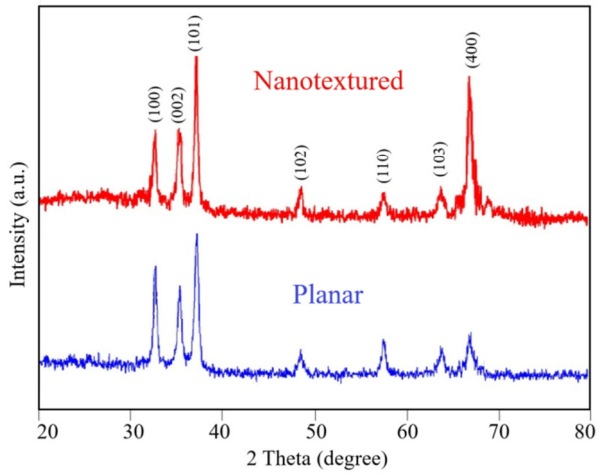

Fig. 2. XRD patterns of ZnO films deposited on planar and nanotextured Si surfaces.

The results of EDS analysis for BS and ZnO films deposited on its surface are illustrated in Figure 3. In the initial state (upper pattern), the main element on the surface is Si, with a minor presence of oxygen (O), indicating the existence of a natural silicon dioxide film on the BS. After the deposition of ZnO (lower pattern), significant changes in the composition are observed. The spectrum clearly shows a peak corresponding to zinc (Zn), confirming the successful deposition of ZnO thin films on the BS. An increase in the oxygen concentration further supports its presence in the film, consistent with the expected results. EDS mapping reveals a uniform distribution of Zn across the entire BS surface (not shown here). In both spectra, the concentration of other potential impurities, such as boron from the substrate, and carbon and nitrogen from the air, is below the detection limit of the EDS method (1 at. %).

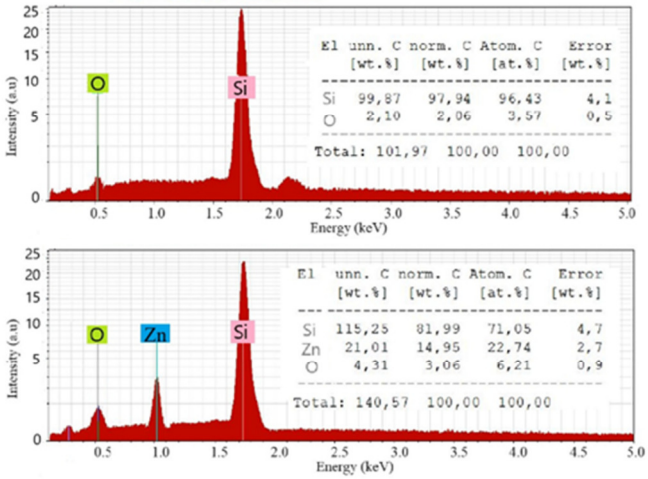

Fig. 3. EDS patterns of BS (upper) and ZnO films deposited on its surface (lower).

The semi-logarithmic I-V characteristics of planar and nanotextured ZnO/Si samples, measured at room temperature in the dark over a DC voltage range of –2 to +2 V, are shown in Figure 4. The inset illustrates the measurement scheme. The obtained curves are representative and correspond to the average values measured across the surface of the samples.

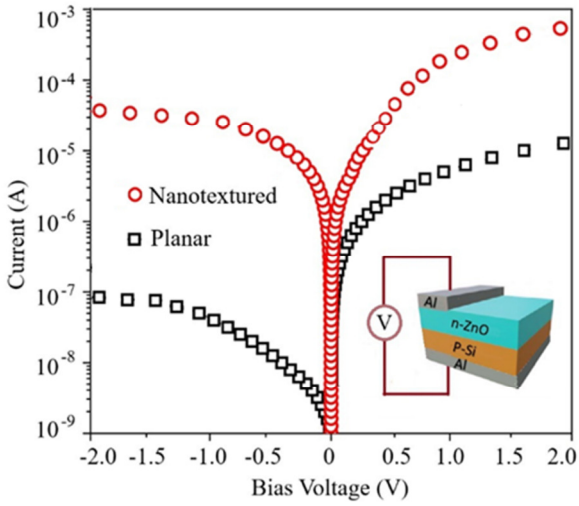

Fig. 4. Semi-logarithmic I-V characteristics of planar and nanotextured ZnO/Si samples. The inset illustrates the measurement scheme.

The studied samples are heterostructures composed of an n-type ZnO film and a p-type (BS)Si substrate. Their electrical parameters can be determined from the obtained I-V characteristics using the Shockley equation, which is based on the thermionic emission model [24]:

$$I = I_0\left[e^{(qV/nkT)} - 1\right] \quad (1)$$

$$\varphi_b = \frac{kT}{q} ln\left(\frac{AA^*T^2}{I_0}\right) \quad (2)$$

where q is the electronic charge, k is Boltzmann's constant, T is the operating temperature, n is the ideality factor, I_0 is the reverse saturation current, φ_b is the apparent potential barrier height at zero bias, A and A^* are the contact area and effective Richardson constant (for undoped ZnO $A^* \sim 32$ A·cm^2·K^2), respectively.

The values of the main electrical parameters of both samples are summarized in Table I.

TABLE I. ELECTRICAL PARAMETERS OF PLANAR AND NANOTEXTURED SAMPLES

Parameters	Planar	Nanotextured
Turn-on voltage (V)	0.5	0.62
Ideality factor	2.3	3.1
Rectification Ratio at ±2V	110	23
Reverse saturation current (A)	$7.26 \cdot 10^{-7}$	$5.11 \cdot 10^{-5}$
Barrier height (eV)	0.75	0.64

Both n-ZnO/p-Si heterostructures exhibit nonlinear rectifying behavior in I-V characteristics (Figure 4), which is attributed to the formation of a potential barrier at the heterojunction interface. However, significant differences in their electrical properties are observed. For nanotextured samples, the measured current at zero, forward, and reverse bias is significantly higher compared to planar samples. Nanotexturing also increases the turn-on voltage, a reduction in the potential barrier height, and decreases the rectification ratio (Table I). The higher forward current suggests reduced contact resistance and enhanced charge transport across the heterojunction. However, the increased reverse current is associated with a higher density of defects and surface states at the interface, which promote the recombination of minority carriers and reduce their lifetime. To mitigate such losses, modern solar cells with a BS front surface often employ passivation coatings [19, 21]. Thus, while nanotexturing can improve certain aspects of charge transport, it also necessitates careful control of surface quality to minimize the negative effects caused by defects and recombination.

The spectral responsivity is an important photoelectric parameter to reflect the performance of a heterostructure to the irradiated photon, which can be defined as:

$$R = I_{ph}/P_{in} \quad (3)$$

where I_{ph} is the response photocurrent, and P_{in} is the incoming optical power.

Figure 5 illustrates the spectral responsivity of n-ZnO/p-Si and n-ZnO/(BS)p-Si heterostructures at a reverse bias of 2 V. Both samples exhibit a broad spectral response across the wavelength range of 350–1000 nm. Two distinct photoresponse peaks are observed: the first peak is located at approximately 370 nm, corresponding to photons absorbed within the bandgap of the ZnO film, and the second peak appears at 860 nm, corresponding to the absorption edge of Si. The presence of BS at the interface enhances the spectral response across the entire range compared to the planar surface. The highest recorded responsivity for the nanostructured samples is 1.15 A/W at 860 nm, which is nearly twice as high as that of planar heterostructures. Comparative studies further indicate that nanotextured BS-based heterostructures universally surpass microtextured porous Si designs in responsivity, irrespective of the ZnO deposition technique (pulsed laser, chemical bath, electrochemical, or hydrothermal) [7, 13–15].

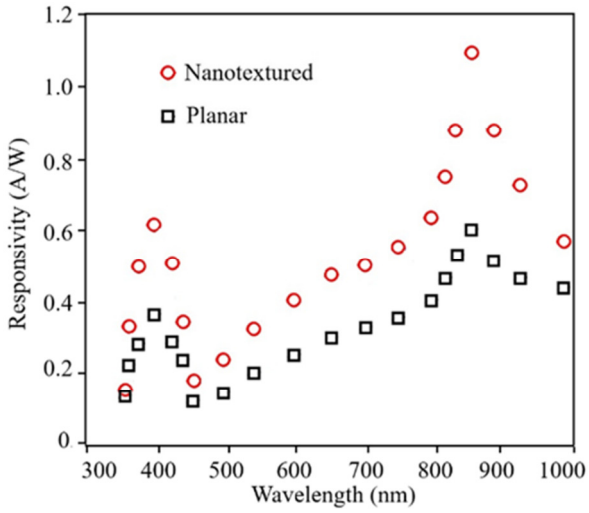

Fig. 5. Spectral responsivity of nanotextured and planar heterostructures.

The improved broadband photoresponse of the nanotextured samples can be attributed to several factors. First, BS exhibits high light-trapping efficiency due to its graded refractive index and the scattering of incident light by the nanoneedles [17], which promotes the intense generation of electron-hole pairs in Si. Second, the nanotextured samples have a significantly larger contact area between ZnO and Si compared to planar heterostructures. This leads to increased carrier collection efficiency and, consequently, a higher photoresponse. Thus, the optimized junction properties, which combine efficient light trapping and improved carrier collection, result in enhanced photoresponse of the nanotextured samples. These findings demonstrate the potential of nanotextured n-ZnO/p-Si heterostructures for use in photonic devices, such as photodetectors, optical sensors, and other optoelectronic applications.

IV. CONCLUSION

In this work, zinc oxide (ZnO) films were deposited on planar and nanotextured silicon (Si) substrates using the sol-gel spin-coating method. The nanotexturing of the Si surface was achieved through the Reactive Ion Etching (RIE) method in the Black Silicon (BS) formation mode, resulting in the creation of an array of conical nanoneedles. Scanning Electron Microscopy (SEM) images and Energy-Dispersive X-ray Spectroscopy (EDS) analysis revealed a uniform and homogeneous distribution of ZnO on the BS nanoneedles. It was observed that the ZnO films deposited on the nanotextured surface exhibit a fibrous structure, attributed to the omnidirectional growth of ZnO crystallites along the nanoneedles. X-ray Diffraction (XRD) confirmed the formation of a polycrystalline hexagonal wurtzite structure of ZnO on both types of substrates. Measurements of the current-voltage

(I–V) characteristics of the fabricated n-ZnO/p-Si heterostructures demonstrated that the nanotextured samples exhibit a higher forward current, indicating improved charge transfer across the heterojunction. However, an increase in the reverse current and a reduction in the potential barrier height highlight the need for further optimization of surface quality to minimize recombination losses. The spectral responsivity of the nanotextured samples in the 350–1000 nm range was significantly higher than that of planar structures, which is attributed to enhanced light trapping and an increased contact area between ZnO and Si. These results underscore the potential of nanotextured n-ZnO/p-Si heterostructures for use in photonic devices.

ACKNOWLEDGMENT

This work was supported by the Science Committee of the Republic of Armenia (research projects no. 21AG-2B011 and 25RG-2B010).

REFERENCES

[1] S. Vyas, "A Short Review on Properties and Applications of Zinc Oxide Based Thin Films and Devices: ZnO as a promising material for applications in electronics, optoelectronics, biomedical and sensors," *Johnson Matthey Technology Review*, vol. 64, no. 2, pp. 202–218, Apr. 2020, https://doi.org/10.1595/205651320X15694993568524.

[2] D. K. Sharma, S. Shukla, K. K. Sharma, and V. Kumar, "A review on ZnO: Fundamental properties and applications," *Materials Today: Proceedings*, vol. 49, pp. 3028–3035, 2022, https://doi.org/10.1016/j.matpr.2020.10.238.

[3] A. Mir, N. Becheikh, L. Khezami, M. Bououdina, and A. Ouderni, "Synthesis, Characterization, and Study of the Photocatalytic Activity upon Polymeric-Surface Modification of ZnO Nanoparticles," *Engineering, Technology & Applied Science Research*, vol. 13, no. 6, pp. 12047–12053, Dec. 2023, https://doi.org/10.48084/etasr.6373.

[4] M. M. Nadareishvili, G. Mamniashvili, D. Jishiashvili, G. Abramishvili, C. Ramana, and J. Ramsden, "Investigation of the Visible Light-Sensitive ZnO Photocatalytic Thin Films," Engineering, Technology & Applied Science Research, vol. 10, no. 2, pp. 5524–5527, Apr. 2020, https://doi.org/10.48084/etasr.3392.

[5] F. Morales-Morales, L. Martínez-Ayala, M. R. Jiménez-Vivanco, and H. Gómez-Pozos, "ZnO Deposition on Silicon and Porous Silicon Substrate via Radio Frequency Magnetron Sputtering," *Coatings*, vol. 13, no. 11, Oct. 2023, Art. no. 1839, https://doi.org/10.3390/coatings13111839.

[6] P. Hazra, S. K. Singh, and S. Jit, "Impact of surface morphology of Si substrate on performance of Si/ZnO heterojunction devices grown by atomic layer deposition technique," *Journal of Vacuum Science & Technology A: Vacuum, Surfaces, and Films*, vol. 33, no. 1, Jan. 2015, Art. no. 01A114, https://doi.org/10.1116/1.4900719.

[7] A. J. Hadi, U. M. Nayef, F. A.-H. Mutlak, and M. S. Jabir, "High-Efficiency Photodetectors Based on Zinc Oxide Nanostructures on Porous Silicon Grown by Pulsed Laser Deposition," *Plasmonics*, vol. 19, no. 2, pp. 577–593, Apr. 2024, https://doi.org/10.1007/s11468-023-02016-3.

[8] C. M. Vlăduț, O.-C. Mocioiu, and E. M. Soare, "Coinage Metals Doped ZnO Obtained by Sol-Gel Method—A Brief Review," *Gels*, vol. 9, no. 5, May 2023, Art. no. 424, https://doi.org/10.3390/gels9050424.

[9] H. Khmissi, B. Azeza, M. Bouzidi, and Z. Al-Rashidi, "Investigation of an Antireflective Coating System for Solar Cells based on Thin Film Multilayers," *Engineering, Technology & Applied Science Research*, vol. 14, no. 3, pp. 14374–14379, Jun. 2024, https://doi.org/10.48084/etasr.7375.

[10] M. Benhaliliba, "A rectifying Al/ZnO/pSi/Al heterojunction as a photodiode," *Micro and Nanostructures*, vol. 163, Mar. 2022, Art. no. 107140, https://doi.org/10.1016/j.spmi.2021.107140.

[11] M. Benhaliliba, "ZnO a multifunctional material: Physical properties, spectroscopic ellipsometry and surface examination," *Optik*, vol. 241, Sep. 2021, Art. no. 167197, https://doi.org/10.1016/j.ijleo.2021.167197.

[12] A. M. Mouafki, F. Bouaïcha, A. Hedibi, and A. Gueddim, "Porous Silicon Antireflective Coatings for Silicon Solar Cells," *Engineering, Technology & Applied Science Research*, vol. 12, no. 2, pp. 8354–8358, Apr. 2022, https://doi.org/10.48084/etasr.4803.

[13] N. Rosli, M. M. Halim, K. M. Chahrour, and M. R. Hashim, "Incorporation of Zinc Oxide on Macroporous Silicon Enhanced the Sensitivity of Macroporous Silicon MSM Photodetector," *ECS Journal of Solid State Science and Technology*, vol. 9, no. 10, Nov. 2020, Art. no. 105005, https://doi.org/10.1149/2162-8777/abc6ef.

[14] S. S. Khudiar, F. A.-H. Mutlak, and U. M. Nayef, "Synthesis of ZnO nanostructures by hydrothermal method deposited on porous silicon for photo-conversion application," *Optik*, vol. 247, Dec. 2021, Art. no. 167903, https://doi.org/10.1016/j.ijleo.2021.167903.

[15] B. P. Bisht, V. Toutam, and S. R. Dhakate, "Self-powered, wide spectral UV response out-of-plane photodetector based on ZnO/porous silicon heterostructure," *Nanotechnology*, vol. 35, no. 18, Apr. 2024, Art. no. 185505, https://doi.org/10.1088/1361-6528/ad14b3.

[16] F. Morales–Morales *et al.*, "Study of zinc oxide/porous silicon interface for optoelectronic devices," *Materials Science in Semiconductor Processing*, vol. 148, Sep. 2022, Art. no. 106810, https://doi.org/10.1016/j.mssp.2022.106810.

[17] S. Wang *et al.*, "An Artificial-Intelligence-Assisted Investigation on the Potential of Black Silicon Nanotextures for Silicon Solar Cells," *ACS Applied Nano Materials*, vol. 5, no. 8, pp. 11636–11647, Aug. 2022, https://doi.org/10.1021/acsanm.2c02619.

[18] G. Ayvazyan, K. Ayvazyan, L. Hakhoyan, and X. Liu, "Properties of Black Silicon Layers Fabricated by Different Techniques for Solar Cell Applications," *physica status solidi (RRL) – Rapid Research Letters*, vol. 18, no. 3, Mar. 2024, Art. no. 2300410, https://doi.org/10.1002/pssr.202300410.

[19] Z. Fan *et al.*, "Recent Progress of Black Silicon: From Fabrications to Applications," *Nanomaterials*, vol. 11, no. 1, Dec. 2020, Art. no. 41, https://doi.org/10.3390/nano11010041.

[20] J. Soueiti, R. Sarieddine, H. Kadiri, A. Alhussein, G. Lerondel, and R. Habchi, "A review of cost-effective black silicon fabrication techniques and applications," *Nanoscale*, vol. 15, no. 10, pp. 4738–4761, 2023, https://doi.org/10.1039/D2NR06087F.

[21] G. Y. Ayvazyan, D. L. Kovalenko, M. S. Lebedev, L. A. Matevosyan, and A. V. Semchenko, "Investigation of the Structural and Optical Properties of Silicon-Perovskite Structures with a Black Silicon Layer," *Journal of Contemporary Physics (Armenian Academy of Sciences)*, vol. 57, no. 3, pp. 274–279, Sep. 2022, https://doi.org/10.1134/S1068337222030069.

[22] G. Ayvazyan, L. Hakhoyan, A. Vardanyan, H. Savin, and X. Liu, "Wetting Properties of Black Silicon Layers Fabricated by Different Techniques," *physica status solidi (RRL) – Rapid Research Letters*, vol. 18, no. 8, Aug. 2024, Art. no. 2400072, https://doi.org/10.1002/pssr.202400072.

[23] Z. Ying *et al.*, "Monolithic perovskite/black-silicon tandems based on tunnel oxide passivated contacts," *Joule*, vol. 6, no. 11, pp. 2644–2661, Nov. 2022, https://doi.org/10.1016/j.joule.2022.09.006.

[24] S. M. Faraz, W. Shah, N. U. H. Alvi, O. Nur, and Q. U. Wahab, "Electrical Characterization of Si/ZnO Nanorod PN Heterojunction Diode," *Advances in Condensed Matter Physics*, vol. 2020, pp. 1–9, Apr. 2020, https://doi.org/10.1155/2020/6410573.